Article

Self-Assembly of Flexible Supramolecular Metallacyclic Ensembles: Structures and Adsorption Properties of Their Nanoporous Crystalline Frameworks

Biswaroop Chatterjee, Juan C. Noveron, Marino J. E. Resendiz, Jie Liu, Takuya Yamamoto, Daniel Parker, Martin Cinke, Cattien V. Nguyen, Atta M. Arif, and Peter J. Stang

J. Am. Chem. Soc., **2004**, 126 (34), 10645-10656• DOI: 10.1021/ja0388919 • Publication Date (Web): 10 August 2004

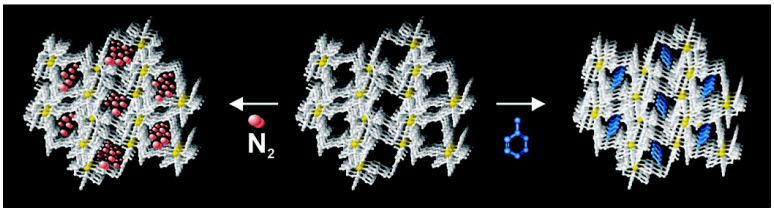

J|A|C|S
ARTICLES
Published on Web 08/10/2004

Self-Assembly of Flexible Supramolecular Metallacyclic Ensembles: Structures and Adsorption Properties of Their Nanoporous Crystalline Frameworks

Biswaroop Chatterjee,[†] Juan C. Noveron,*[,‡] Marino J. E. Resendiz,[†] Jie Liu,[†] Takuya Yamamoto,[†] Daniel Parker,[†] Martin Cinke,[§] Cattien V. Nguyen,[§] Atta M. Arif,[†] and Peter J. Stang*[,†]

Contribution from the Department of Chemistry, University of Utah, Salt Lake City, Utah 84112, Department of Chemistry, University of Texas at El Paso, El Paso, Texas 79968, and Eloret Corporation, NASA Ames Research Center, Moffett Field, California 94035

Received October 6, 2003; E-mail: jcnoveron@utep.edu; stang@chem.utah.edu

Abstract: The syntheses, structures, and N_2 adsorption properties of six new supramolecular metallacycles are reported. Flexible ditopic linkers, **1**−**4**, with systematically varied lengths and conformational degrees of freedom were synthesized utilizing ester linkages. They were used in combination with (dppp)M(OTf)$_2$, where M = Pt(II) and Pd(II), and *cis*-(Me$_3$P)$_2$Pt(OTf)$_2$ to form flexible supramolecular metallacycles **5**−**10** in 88−98% isolated yields. Their structures were characterized via multinuclear NMR and X-ray crystallography. The metallacycles stack to form porous structures in the crystalline state. The pore dimensions depend on both the phosphorus ligands attached to the metals and the flexible linkers. Adsorption studies on the porous materials show that **5a**, **6**, **8**, and **9** held 11.7, 16.5, 5.7, and 6.8 cm^3/g STP of N_2 at 77 K, respectively. A guest-exchange study with nitromethane and toluene reveals that the nanopore in **5** is flexible, a property which was transferred from the linker to the supramolecular structure in the solid state.

Introduction

The use of coordination-directed self-assembly is now an established methodology for the synthesis of discrete molecular species.[1] This approach offers a variety of opportunities for the preparation of nanoscopic supramolecular ensembles of predetermined shape, size, and symmetry. For example, numerous triangular[2] and quadrangular[3] two-dimensional assemblies as well as three-dimensional ensembles including Platonic[4] and Archimedean[5] polyhedra, adamantanoids,[6] boxes,[7] prisms,[8] and tetragonal architectures[9] have been reported. The ability to modify the organic components of frameworks also offers unlimited possibilities for the introduction of functionality into nanostructures. For example, substrate binding sites,[10] porphyrin units,[11] Lewis base receptor sites,[12] and shape-selective cavities[8e,9b] have been incorporated within coordination-directed supra-

[†] University of Utah.
[‡] University of Texas at El Paso.
[§] Eloret Corp.

(1) (a) Chambron, J.-C.; Dietrich-Buchecker, C.; Sauvage, J.-P. In *Comprehensive Supramolecular Chemistry*; Lehn, J.-M., Atwood, J. L., Davies, J. E. D., MacNicol, D. D., Vögtle, F., Eds.; Pergamon: Oxford, 1996; Vol. 9, pp 43−83. (b) Leininger, S.; Olenyuk, B.; Stang, P. J. *Chem. Rev.* **2000**, *100*, 853−908. (c) Seidel, S. R.; Stang, P. J. *Acc. Chem. Res.* **2002**, *35*, 972−983. (d) Fujita, M. *Chem. Soc. Rev.* **1998**, *27*, 417−425.
(2) (a) Schweiger, M.; Seidel, S. R.; Arif, A. M.; Stang, P. J. *Inorg. Chem.* **2002**, *41*, 2556−2559. (b) Kryschenko, Y. K.; Seidel, S. R.; Arif, A. M.; Stang, P. J. *J. Am. Chem. Soc.* **2003**, *125*, 5193−5198. (c) Piotrowski, H.; Polborn, K.; Hilt, G.; Severin, K. *J. Am. Chem. Soc.* **2001**, *123*, 2699−2700. (d) Sautter, A.; Schmid, D. G.; Jung, G.; Würthner, F. *J. Am. Chem. Soc.* **2001**, *123*, 5424−5430. (e) Cotton, F. A.; Lin, C.; Murillo, C. A. *Inorg. Chem.* **2001**, *40*, 575−577.
(3) (a) Pak, J. J.; Greaves, J.; McCord, D. J.; Shea, K. J. *Organometallics* **2002**, *21*, 3552−3561. (b) Lee, S. J.; Lin, W. *J. Am. Chem. Soc.* **2002**, *124*, 4554−4555. (c) Liu, X.; Stern, C. L.; Mirkin, C. A. *Organometallics* **2002**, *21*, 1017−1019. (d) Han, G.; Dong, G.; Duan, C.-Y.; Mo, H.; Meng, Q.-j. *New J. Chem.* **2002**, *26*, 1371−1377. (e) Cotton, F. A.; Lin, C.; Murillo, C. A. *J. Am. Chem. Soc.* **2001**, *123*, 2670−2671.
(4) (a) Johannessen, S. C.; Brisbois, R. G.; Fischer, J. P.; Grieco, P. A.; Counterman, A. E.; Clemmer, D. E. *J. Am. Chem. Soc.* **2001**, *123*, 3818−3819. (b) Olenyuk, B.; Levin, M. D.; Whiteford, J. A.; Shield, J. E.; Stang, P. J. *J. Am. Chem. Soc.* **1999**, *121*, 10434−10435. (c) Parac, T. N.; Caulder, D. L.; Raymond, K. N. *J. Am. Chem. Soc.* **1998**, *120*, 8003−8004. (d) Ibukuro, F.; Kusukawa, T.; Fujita, M. *J. Am. Chem. Soc.* **1998**, *120*, 8561−8562. (e) Fujita, M.; Oguro, D.; Miyazawa, M.; Oka, H.; Yamaguchi, K.; Ogura, K. *Nature* **1995**, *378*, 469−471.
(5) (a) Leininger, S.; Fan, J.; Schmitz, M.; Stang, P. J. *Proc. Natl. Acad. Sci. U.S.A.* **2000**, *97*, 1380−1384. (b) Olenyuk, B.; Whiteford, J. A.; Fechtenkötter, A.; Stang, P. J. *Nature* **1999**, *398*, 796−799.
(6) (a) Schweiger, M.; Seidel, S. R.; Schmitz, M.; Stang, P. J. *Org. Lett.* **2000**, *2*, 1255−1257. (b) Saalfrank, R. W.; Burak, R.; Breit, A.; Stalke, D.; Herbst-Irmer, R.; Daub, J.; Porsch, M.; Bill, E.; Müther, M.; Trautwein, A. X. *Angew. Chem.* **1994**, *106*, 1697−1699. (c) Saalfrank, R. W.; Hörner, B.; Stalke, D.; Salbeck, J. *Angew. Chem.* **1993**, *105*, 1223−1225.
(7) (a) Yamanoi, Y.; Sakamoto, Y.; Kusukawa, T.; Fujita, M.; Sakamoto, S.; Yamaguchi, K. *J. Am. Chem. Soc.* **2001**, *123*, 980−981. (b) Aoyagi, M.; Biradha, K.; Fujita, M. *J. Am. Chem. Soc.* **1999**, *121*, 7457−7458.
(8) (a) Kuehl, C. J.; Kryschenko, Y. K.; Radhakrishnan, U.; Seidel, S. R.; Huang, S. D.; Stang, P. J. *Proc. Natl. Acad. Sci. U.S.A.* **2002**, *99*, 4932−4936. (b) Kuehl, C. J.; Yamamoto, T.; Seidel, S. R.; Stang, P. J. *Org. Lett.* **2002**, *4*, 913−915. (c) Hiraoka, S.; Kubota, Y.; Fujita, M. *Chem. Commun.* **2000**, 1509−1510. (d) Liu, H.-K.; Sun, W.-Y.; Ma, D.-J.; Tang, W.-X.; Yu, K.-B. *Chem. Commun.* **2000**, 591−592. (e) Fujita, M.; Nagao, S.; Ogura, K. *J. Am. Chem. Soc.* **1995**, *117*, 1649−1650.
(9) (a) Takeda, N.; Umemoto, K.; Yamaguchi, K.; Fujita, M. *Nature* **1999**, *398*, 794−796. (b) Kusukawa, T.; Fujita, M. *J. Am. Chem. Soc.* **2002**, *124*, 13576−13582. (c) Caulder, D. L.; Raymond, K. N. *J. Chem. Soc., Dalton Trans.* **1999**, 1185−1200. (d) Caulder, D. L.; Raymond, K. N. *Acc. Chem. Res.* **1999**, *32*, 975−982.
(10) (a) Bourgeois, J.-P.; Fujita, M.; Kawano, M.; Sakamoto, S.; Yamaguchi, K. *J. Am. Chem. Soc.* **2003**, *125*, 9260−9261. (b) Kusukawa, T.; Fujita, M. *J. Am. Chem. Soc.* **1999**, *121*, 1397−1398. (c) Fujita, M.; Nagao, S.; Iida, M.; Ogata, K.; Ogura, K. *J. Am. Chem. Soc.* **1993**, *115*, 1574−1576. (d) Sun, S.-S.; Lees, A. J. *J. Am. Chem. Soc.* **2000**, *122*, 8956−8967.

molecular ensembles. Furthermore, when considering that metal-containing structures often possess magnetic, photophysical, and redox properties not accessible from purely organic systems, supramolecular metal−organic assemblies that couple both the functionality of the organic frames and the properties of the inorganic components could have a significant impact in the areas of molecular sensing, catalysis, molecular electronics, and new hydrogen fuel technologies.[13]

Current research directions that apply the edge-directed[1b,c] and the face-directed[1d] strategies for self-assembly have focused on the design and synthesis of rigid molecular components which control the geometry and symmetry of the final ensembles. The use of flexible donor components is less common in self-assembly, and only a handful of examples exist that employ flexible organic linkers to generate discrete structures.[14] Flexible organic components are generally less predictable during self-assembly and have a tendency to generate [2]-catenanes[15] or oligomers[16] upon reaction with metals. They often need guest molecules acting as templates in order to form discrete structures.[14b,15a]

Incorporating flexible linkers into supramolecular systems has several potential advantages. They can generate ensembles in which the flexible nature of the units is reflected in the supramolecule, thus affording nanostructures that can "breathe" in the solid state and exhibit dynamic properties. This is particularly interesting if the flexible groups contain dynamic modes that generate predictable conformational changes in the solid state. Flexible components in self-assembly could potentially "find" conformations that are thermodynamically favorable for host−guest interactions, thus allowing for chemosensing activity in the solid state. These properties are yet to be realized in supramolecular systems; hence, studies that incorporate flexible units in supramolecular ensembles are desirable.

Herein, we report on the self-assembly of six metallacycles from flexible linkers and cis-square-planar metal units. The linkers used are ditopic pyridyl molecules that are systematically varied in length and conformational degrees of freedom: 1,2-ethanediyl di-4-pyridinecarboxylate (**1**), 1,3-propanediyl di-4-pyridinecarboxylate (**2**), 2-butyne-1,4-diyl di-4-pyridinecarboxylate (**3**), and bis(4-pyridylmethyl) pyridine-2,6-dicarboxylate (**4**) (Figure 1). Upon self-assembly with (dppp)$Pt(OTf)_2$, (dppp)-$Pd(OTf)_2$ (where (dppp) = 1,3-bis(diphenylphosphino)propane), and *cis*-$(Me_3P)_2Pt(OTf)_2$, large dimeric metallacycles were formed from **1**−**3**. In the case of **4**, an equilibrium of dimeric and trimeric structures was observed. They were then crystallized and characterized by X-ray crystallography. The metallacycles stack together in the crystalline state, generating nanopores that run along one or two directions of the crystals. Solvent-exchange and N_2 adsorption studies on the porous nature of these materials are reported.

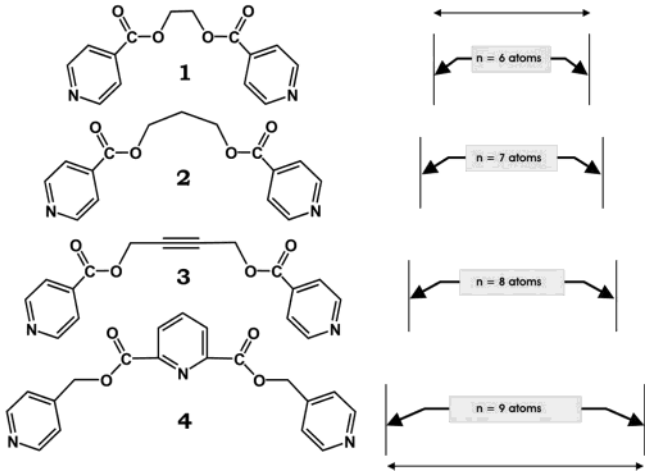

Figure 1. Flexible linkers **1**−**4** used in this study (left) with the number of atoms (*n*) present in the spacer group between the pyridyl moieties (right).

Results

Syntheses of Ditopic Flexible Linkers 1−4. The linkers shown in Figure 1 were prepared according to eqs 1 and 2.

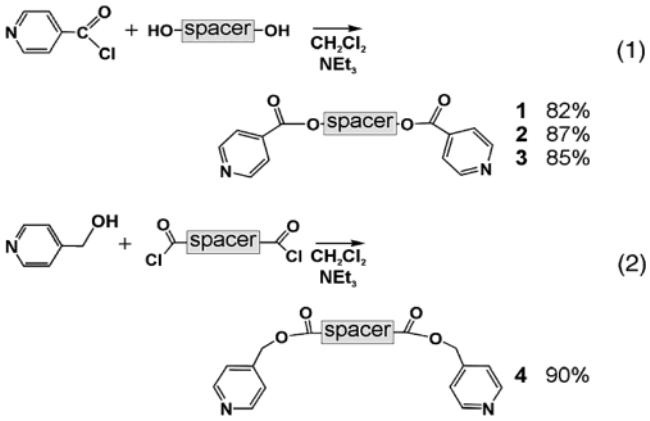

(1)

(2)

Reaction of 2 equiv of isonicotinoyl chloride with the corresponding diol in anhydrous dichloromethane and triethylamine under reflux generated the corresponding products **1**−**3** in good yields (eq 1). Similarly, a 2:1 mixture of 4-pyridinemethanol and 2,6-pyridinedicarboxylic acid chloride generated the ditopic flexible linker **4** with an inverted ester group (eq 2).

Syntheses of Metallacycles 5−10. The discrete metallacyclic complexes **5**−**9** (Figure 2) were prepared when stoichiometric mixtures of the cis-square-planar metal units and the corresponding flexible linkers **1**−**3** were reacted in nitromethane-d_3.

For example, when (dppp)$Pt(OTf)_2$ was combined with an equimolar amount of **1** at room temperature, it resulted in the spontaneous formation of the metallacyclic assembly [(dppp)-$Pt(\mathbf{1})]_2(OTf)_4$ (**5**). The self-assemblies of **6**−**9** were carried out in the same manner. The chemical shift changes of the phosphorus atoms attached to the metals and the α- and β-pyridyl protons of the flexible ligands are indicative of the formation of the self-assemblies. The highly symmetrical nature

(11) (a) Stang, P. J.; Fan, J.; Olenyuk, B. *Chem. Commun.* **1997**, 1453−1454. (b) Drain, C. M.; Lehn, J.-M. *J. Chem. Soc., Chem. Commun.* **1994**, 2313−2315. (c) Fan, J.; Whiteford, J. A.; Olenyuk, B.; Levin, M. D.; Stang, P. J.; Fleischer, E. B. *J. Am. Chem. Soc.* **1999**, *121*, 2741−2752.
(12) (a) Schnebeck, R.-D.; Randaccio, L.; Zangrando, E.; Lippert, B. *Angew. Chem., Int. Ed.* **1998**, *37*, 119−121. (b) Whiteford, J. A.; Lu, C. V.; Stang, P. J. *J. Am. Chem. Soc.* **1997**, *119*, 2524−2533. (c) Whiteford, J. A.; Stang, P. J.; Huang, S. D. *Inorg. Chem.* **1998**, *37*, 5595−5601.
(13) Berry, G. D.; Aceves, S. M. *Energy Fuels* **1998**, *12*, 49−55.
(14) (a) Tabellion, F. M.; Seidel, S. R.; Arif, A. M.; Stang, P. J. *J. Am. Chem. Soc.* **2001**, *123*, 7740−7741. (b) Tabellion, F. M.; Seidel, S. R.; Arif, A. M.; Stang, P. J. *J. Am. Chem. Soc.* **2001**, *123*, 11982−11990.
(15) (a) Fujita, M.; Ibukuro, F.; Ogura, K.; Seki, H.; Kamo, O.; Imanari, M. *J. Am. Chem. Soc.* **1996**, *118*, 899−900. (b) Fujita, M.; Aoyagi, M.; Ibukuro, F.; Ogura, K.; Yamaguchi, K. *J. Am. Chem. Soc.* **1998**, *120*, 611−612. (c) Fujita, M.; Ibukuro, F.; Yamaguchi, K.; Ogura, K. *J. Am. Chem. Soc.* **1995**, *117*, 4175−4176.
(16) (a) Hiraoka, S.; Fujita, M. *J. Am. Chem. Soc.* **1999**, *121*, 10239−10240. (b) Fujita, M.; Kwon, Y. J.; Sasaki, O.; Yamaguchi, K.; Ogura, K. *J. Am. Chem. Soc.* **1995**, *117*, 7287−7288.

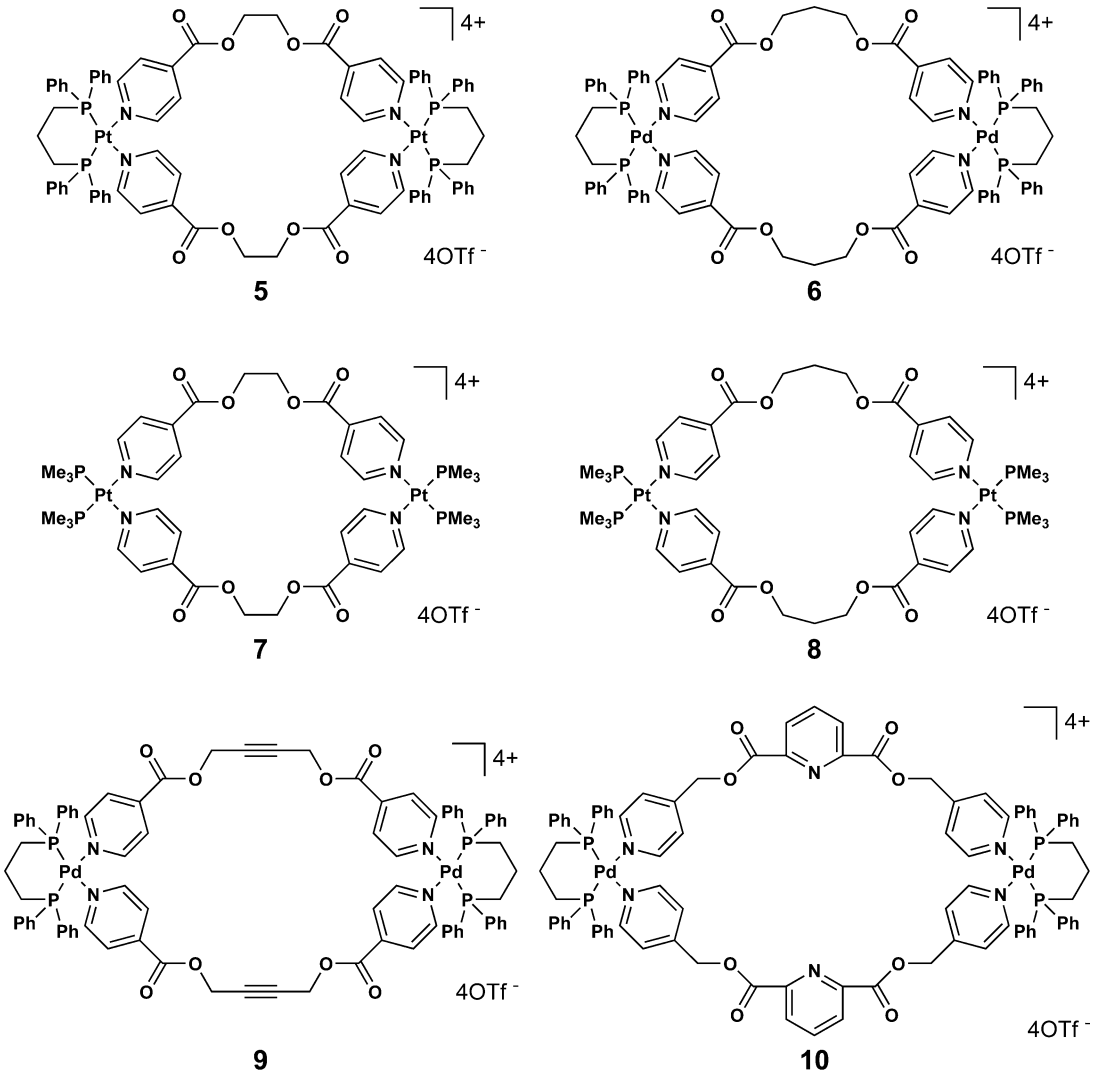

Figure 2. Chemical structures of metallacycles **5**−**10**.

of **5**−**9** in solution is shown by sharp singlet peaks in the ^{31}P-{^{1}H} NMR spectra at δ −13.1, 9.5−9.3, and −27.9 ppm for the metallacycles consisting of (dppp)Pt, (dppp)Pd, and $(Me_3P)_2$-Pt, respectively. The difference in the ^{195}Pt satellite coupling constants of the two types of phosphorus ligands was relatively small: J_{P-Pt} = 3015 Hz for (dppp)Pt, 3150 and 3147 Hz for $(Me_3P)_2$Pt. Well-defined peaks in the ^{1}H NMR spectra were observed for **5**−**9**. The chemical shifts of the α-pyridyl protons (δ 8.88−8.75 ppm) were similar to those of the free linkers, whereas the β-pyridyl protons shifted upfield to δ 7.65−7.54 ppm for the complexes consisting of (dppp)M units. In the case of the reactions with $(Me_3P)_2Pt(OTf)_2$, downfield shifts were observed for both α- and β-pyridyl protons (δ 9.11−9.04 and 8.15−8.09 ppm, respectively). This indicates that the chemical shifts of the α- and β-pyridyl protons depend largely on the phosphorus ligands and less on the metals. The uncoordinated triflate counterions of **5**−**9** exhibit singlet peaks between δ −78.5 and −78.7 ppm in the ^{19}F NMR spectra.

In contrast to the single species formation in the self-assembly of **5**−**9**, equimolar reaction of $(dppp)Pd(OTf)_2$ with ligand **4** in nitromethane-d_3 at room temperature generated an equilibrium of two structures. ESI-MS indicates that the two species were dimeric $[(dppp)Pd(\mathbf{4})]_2(OTf)_4$ and trimeric $[(dppp)Pd(\mathbf{4})]_3(OTf)_6$. Isotopically resolved peaks were found at m/z = 2183.0 and 1600.3 for $\{[(dppp)Pd(\mathbf{4})]_2(OTf)_3\}^+$ and $\{[(dppp)Pd(\mathbf{4})]_3(OTf)_4\}^{2+}$, respectively. The ^{31}P{^{1}H} NMR spectrum of the reaction mixture was indicative of two highly symmetrical species, as shown by two sharp singlet peaks at δ 10.8 and 9.3 ppm. Similarly, two sets of signals were observed in the ^{1}H NMR spectrum, whereas only one singlet appeared at δ −78.6 ppm in the ^{19}F NMR spectrum. However, upon crystallization, only the dimeric structure $[(dppp)Pd(\mathbf{4})]_2(OTf)_4$ (**10**) was obtained (Figure 2).

Crystal Structures of Metallacycles 5a, 5b, and 6−**10.** X-ray-quality crystals of **5a**, **7**, **8**, and **10** were obtained by diethyl ether diffusion into solutions of the corresponding compounds in nitromethane. When **5a** was recrystallized from a mixture of dichloromethane and toluene (90:10), a new host−guest complex of **5** + toluene (**5b**) was obtained. Metallacycles **6** and **9** were crystallized by diethyl ether diffusion into methanol solution of the assemblies. The crystal structures of **5a**, **5b**, and **6**−**10** are shown in Figures 3−9. Their crystallographic parameters are shown in Table 1, and relevant bond lengths and bond angles are summarized in Table 2.

The crystal structures of the metallacycles **5a**, **5b**, and **6**−**10** reveal interesting trends depending on the metal (Pt or Pd), P ligand, (dppp) or $(Me_3P)_2$, and N linker (flexible linkers, **1**−**4**) used (Table 2). As expected, the metal-to-metal distance (M−

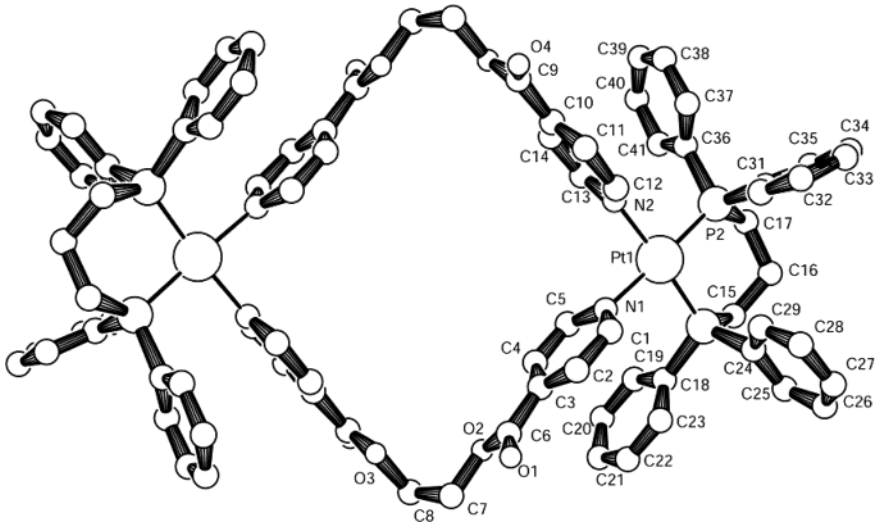

Figure 3. Crystal structure of **5a**. Hydrogen atoms, solvent molecules, and counterions are omitted for clarity. Metallacycle **5**, $[(dppp)Pt(\mathbf{1})]_2(OTf)_4$, incorporated six nitromethane molecules (omitted) to form **5a**; $\pi-\pi$ stacking interactions are observed between the pyridyl groups of the linker and the two phenyl groups of the (dppp) moiety.

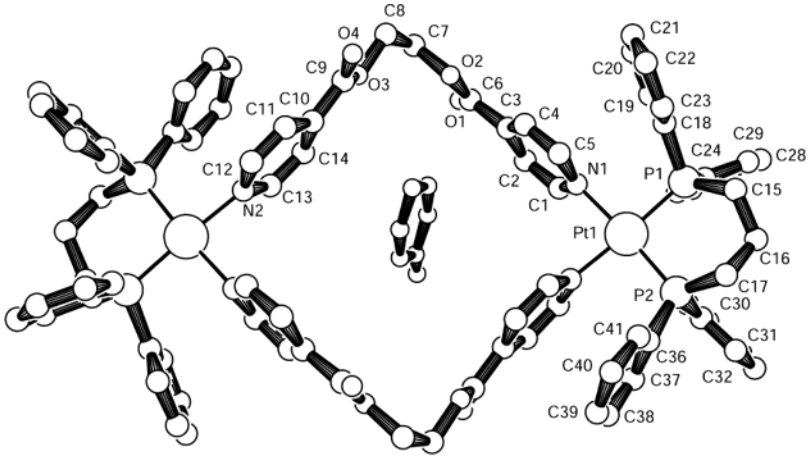

Figure 4. Crystal structure of **5b** incorporating a toluene guest. Hydrogen atoms and counterions are omitted for clarity. In the solid state, $\pi-\pi$ stacking interactions are observed between the pyridyl groups of the linker and the two phenyl groups of the (dppp) moiety as well as between the pyridyl group and the incorporated toluene molecule.

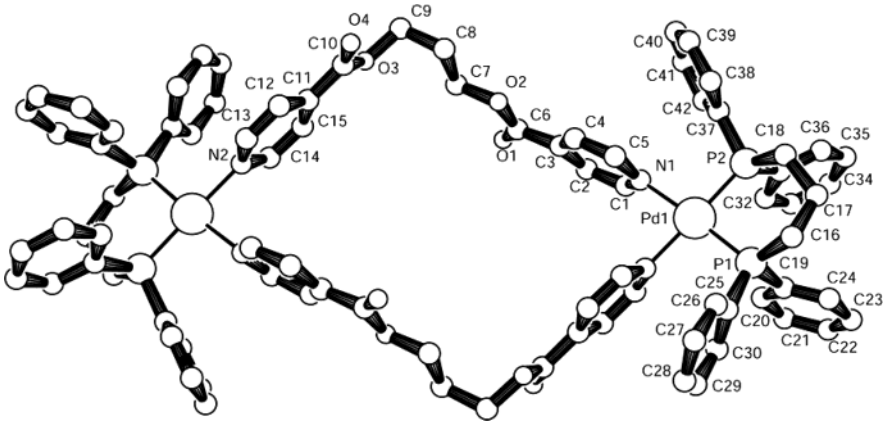

Figure 5. Crystal structure of **6**. Hydrogen atoms, solvent molecules, and counterions are omitted for clarity. In the solid state, $\pi-\pi$ stacking interactions are observed between the pyridyl groups of the linker and the two phenyl groups of the (dppp) moiety.

M) in each metallacycle increases as the length of the N linker increases within the same P ligand series except for **10**; i.e., M−M increases as **5a** = 12.3 Å, **5b** = 12.7 Å, **6** = 15.0 Å, **9** = 15.4 Å, and for **7** = 14.2 Å, **8** = 14.7 Å. However, ensemble **10**, with the longest linker, has a constricted cavity in the solid state (M−M = 8.8 Å). The ethanediyl groups in the crystal structures of **5a**, **5b**, and **7** can adopt two possible conformations, trans (*T*) and gauche (*G*), for O(2)−C(7)−C(8)−O(3). This can also be applied to O(2)−C(7)−C(10)−O(3) in the crystal structure of **9** by considering that the four-carbon unit C(7)−

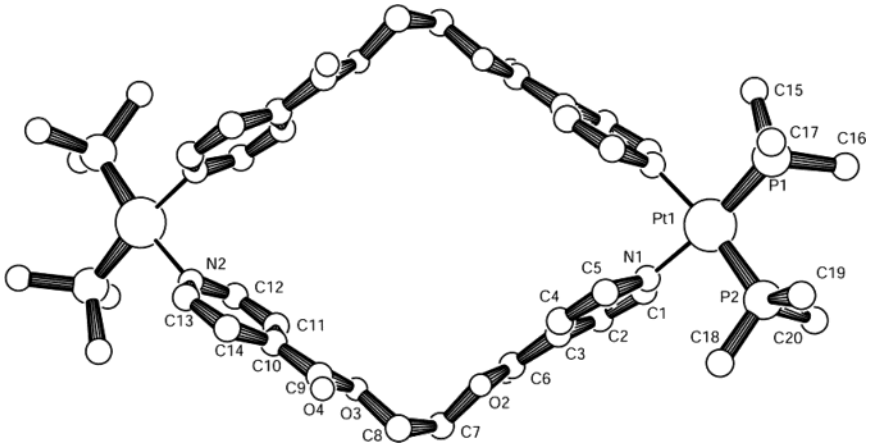

Figure 6. Crystal structure of **7**. Hydrogen atoms, solvent molecules, and counterions are omitted for clarity.

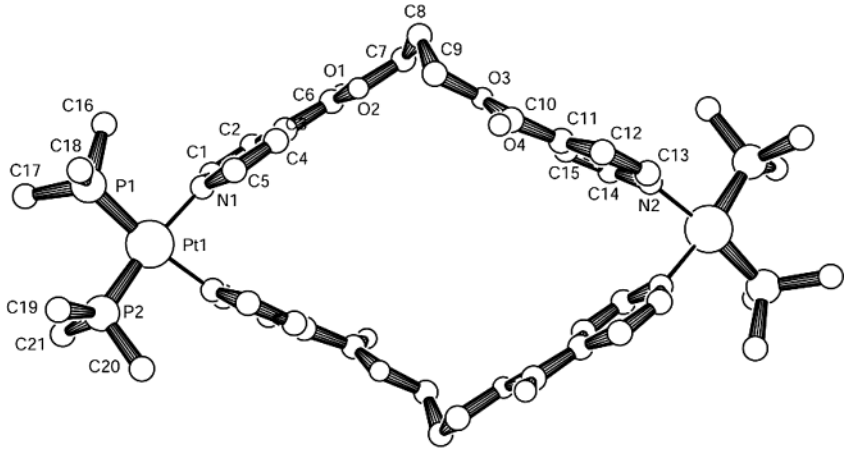

Figure 7. Crystal structure of **8**. Hydrogen atoms, solvent molecules, and counterions are omitted for clarity.

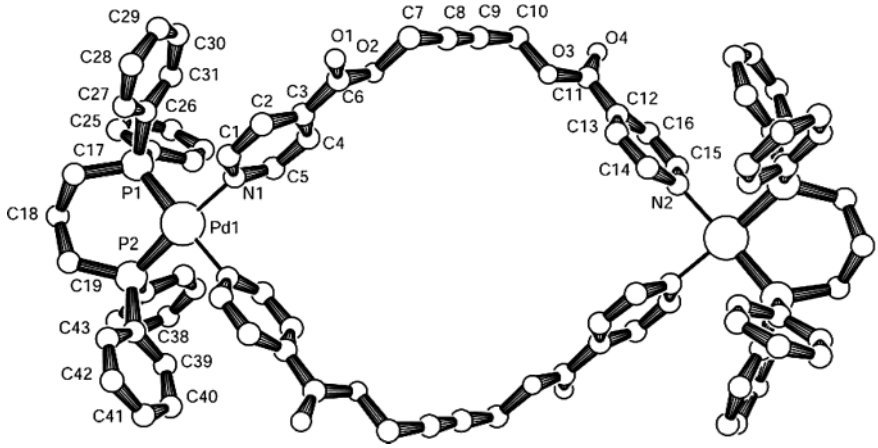

Figure 8. Crystal structure of **9**. Hydrogen atoms, solvent molecules, and counterions are omitted for clarity. In the solid state, $\pi-\pi$ stacking interactions are observed between the pyridyl groups of the linker and the two phenyl groups of the (dppp) moiety.

C(8)−C(9)−C(10) is almost straight. In the case of **6** and **8**, the propanediyl group has four possible conformations, *TT*, *GT*, *GG*, and *GG′*,[17] for O(2)−C(7)−C(8)−C(9) and C(7)−C(8)−C(9)−O(3). All the N linkers in **5a**, **5b**, and **7**−**9** are in the gauche conformation. Interestingly, the conformations in **6** are gauche and trans (*GT*), whereas the $(Me_3P)_2Pt$ counterpart **8** has two gauche conformations (*GG*).

(17) Carlucci, L.; Ciani, G.; v. Gundenberg, D. W.; Proserpio, D. M. *Inorg. Chem.* **1997**, *36*, 3812−3813.

The geometries at the square-planar metals are also notable. Although all the metallacycles have identical bond lengths of M−P (2.3 Å) and M−N (2.1 Å), the angles in the square-planar Pt and Pd are quite different. The (dppp)Pt of **5a** and **5b** and the (dppp)Pd of **9** and **10** have similar angular distributions. For these species the angles of P(1)−M−P(2) and N(1)−M−N(2) range from 91.3 to 92.7° and from 85.6 to 86.3° respectively. On the other hand, the complexes **7** and **8** have larger P(1)−M−P(2) (96.1°) but smaller N(1)−M−N(2) (81.1−

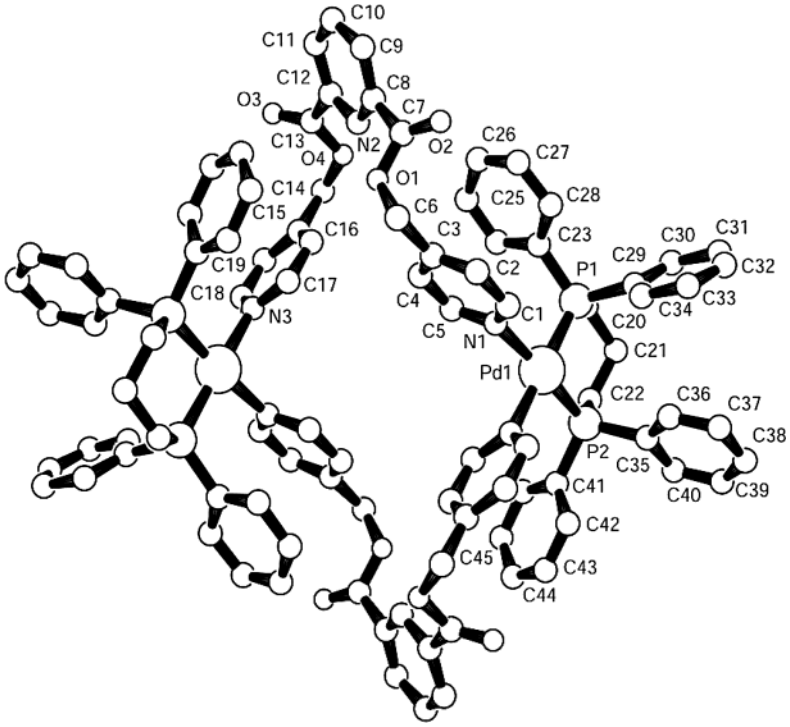

Figure 9. Crystal structure of **10**. Hydrogen atoms, solvent molecules, and counterions are omitted for clarity. A constricted cavity is observed. In the solid state, $\pi-\pi$ stacking interactions are observed between the pyridyl groups of the linker and the two phenyl groups of the (dppp) moiety.

Table 1. Crystal Data for **5a**, **5b**, and **6**−**10**

	5a	5b	6	7	8	9	10
empirical formula	C92 H94 F12 N10 O32 P4 Pt2 S4	C97 H89 F12 N4 O20 P4 Pt2 S4	C90 H92 F12 N4 O24 P4 Pd2 S4	C45 H63 F12 N5 O22 P4 Pt2 S4	C50 H74 F12 N4 O21 P4 Pt2 S4	C91 H80 F12 N4 O21 P4 Pd2 S4	C98 H88 F12 N8 O24 P4 Pd2 S4
formula weight	2722.07	2501.02	2306.60	1896.30	1937.43	2258.51	2454.68
space group	$P2_1/n$	$P2_1/n$	$P\bar{1}$	$P\bar{1}$	$P\bar{1}$	$P2_1/n$	$P\bar{1}$
unit cell dimensions							
a, Å	13.6056(3)	13.2388(3)	10.5043(2)	8.81510(10)	8.8035(2)	12.8418(3)	11.7834(2)
b, Å	23.3073(4)	24.2168(5)	12.0394(3)	9.03470(10)	9.1015(2)	28.6558(7)	15.3708(3)
c, Å	19.1246(4)	19.0150(4)	20.2334(6)	22.8904(4)	23.3350(7)	14.1269(4)	15.4053(3)
α, °	90	90	91.9466(10)	90.8881(6)	89.8587(7)	90	88.4998(8)
β, °	105.4608(10)	106.8891(11)	104.8438(12)	91.5730(6)	88.1624(8)	105.4719(10)	81.9321(8)
γ, °	90	90	90.2628(20)	99.6842(6)	80.5377(16)	90	70.4728(13)
volume, Å^3	5845.1(2)	5833.3(2)	2471.77(11)	1796.00(4)	1843.32(8)	5010.2(2)	2603.06(8)
independent reflctns	10 604	13 219	9915	8054	8082	11 291	11 811
goodness-of-fit on F^2	1.116	1.086	1.016	1.187	1.054	1.033	1.027
final *R* indices							
[$I > 2\sigma(I)$]: *R*1,[a] w*R*2[b]	0.0652, 0.1650	0.0812, 0.1872	0.0551, 0.1242	0.0510, 0.1217	0.0429, 0.0938	0.0690, 0.1619	0.0615, 0.1384

[a] $R1 = \sum(||F_o| - |F_c||)/\sum|F_o|$. [b] $wR2 = [\sum(w(F_o^2 - F_c^2)^2)/\sum(F_o^2)^2]^{1/2}$.

81.4°) angles. This is likely caused by the $\pi-\pi$ staking interaction of the phenyl groups of the (dppp) ligands and the pyridyl groups of the N linkers (Figures 3, 4, 8, and 9). This interaction "pulls" the pyridyl groups outward, resulting in the larger N(1)−M−N(2) angle in **5a**, **5b**, **9**, and **10** compared to those of the $(Me_3P)_2Pt$ systems (**7** and **8**). Consequently, relatively small angles of P(1)−M−P(2) for **5a**, **5b**, **9**, and **10** are observed compared to those in **7** and **8**. The P−M−N angles are also similar throughout these complexes **5a**, **5b**, and **7**−**10**. The square-planar geometry at the Pd center in **6** is different from that in the others, although it has a similar $\pi-\pi$ stacking interaction (Figure 5). Both P(1)−M−P(2) (89.0°) and N(1)−M−N(2) (83.3°) angles are noticeably smaller than in the other (dppp)M complexes.

Another interesting differentiation between the (dppp)M and $(Me_3P)_2Pt$ systems is the position of the triflate counterions in the crystal structures of **5a**, **5b**, and **6**−**10**. The counterions were found nearby the positively charged metal centers. One triflate counterion is located on each side of the coordination plane (axial position) of the square-planar metal centers. For the (dppp)M complexes, the closest oxygen atom is found approximately 3 Å away from the metal center on one side of the (dppp)M coordination plane, while on the other side the nearest oxygen atom is significantly farther away (3.9−4.3 Å) (Table 2). In contrast, the closest triflate oxygen atoms are approximately equidistant to the metal centers (3.6−3.9 Å) on either side of the $(Me_3P)_2Pt$ coordination plane in complexes **7** and **8**.

Adsorption Isotherms of Crystals 5a, 6, 8, and 9. Adsorption isotherms with N_2 were measured on desolvated polycrystalline samples **5a**, **6**, **8**, and **9**. The N_2 adsorption experiments were carried out by introducing high-purity grade N_2 gas at 77 K. Isotherm plots and maximum volumes adsorbed for **5a**, **6**, **8**, and **9** are shown in Figure 10 and Table 2, respectively. Desolvated crystals of **6** exhibit the greatest adsorption; 16.5 cm^3 STP of N_2 was adsorbed per gram of **6** at 750 Torr. A

Table 2. Metallacycle and Pore Crystallographic Data for **5a**, **5b**, and **6**−**10** and N_2 Adsorption Data for **5**a, **6**, **8**, and **9**

		5a	5b	6	7	8	9	10
		Metallacycle Crystallographic Data						
M		Pt	Pt	Pd	Pt	Pt	Pd	Pd
P ligand		dppp	dppp	dppp	$(Me_3P)_2$	$(Me_3P)_2$	dppp	dppp
N linker		**1**	**1**	**2**	**1**	**2**	**3**	**4**
M−M (Å)		12.3	12.7	15.0	14.2	14.7	15.4	8.8
N linker−N linker (Å)[a]		12.3	11.9	10.4	9.9	10.6	11.1	12.9
N linker conformation[b]		*G*	*G*	*GT*	*G*	*GG*	*G*	
N linker dihedral angle (°)[b]		73.3	75.6	61.2	90.7	63.5	84.7	
				0.8		67.7		
M−P(1) (Å)		2.3	2.3	2.3	2.3	2.3	2.3	2.3
M−P(2) (Å)		2.3	2.3	2.3	2.3	2.3	2.3	2.3
M−N(1) (Å)		2.1	2.1	2.1	2.1	2.1	2.1	2.1
M−N(2) (Å)[c]		2.1	2.1	2.1	2.1	2.1	2.1	2.1
P(1)−M−P(2) (°)		92.7	92.6	89.0	96.1	96.1	91.7	91.3
N(1)−M−N(2) (°)		86.1	85.6	83.3	81.1	81.4	86.3	85.7
P(1)−M−N (°)[d]		89.5	91.6	93.3	91.3	90.9	91.9	91.4
P(2)−M−N (°)[d]		91.7	90.3	94.5	91.4	91.5	90.1	91.9
M−OTf (Å)[e]	M−O(5)	6.4	4.9	6.4	3.9	4.6	3.9	5.5
	M−O(6)	4.3	5.4	5.4	5.1	3.6	6.1	6.6
	M−O(7)	5.1	3.1	4.1	4.0	3.8	6.1	4.3
	M−O(8)	5.2	5.2	5.1	3.6	4.1	3.0	5.2
	M−O(9)	3.2	4.2	4.8	3.9	5.3	5.1	3.2
	M−O(10)	5.4	6.5	2.9	4.5	3.7	4.9	4.4
		Pore Crystallographic Data						
pore direction by crystallographic axis		*c*	*c*	*a*	*a*, *b*	*a*, *b*	*a*	*a*
metallacycle stacking distance (Å)		19.1	19.0	10.5	8.8, 9.0	8.8, 9.1	12.8	11.8
estimated pore dimension, M−M (Å)		10.8	11.1	8.9	12.6, 12.7	13.0, 13.1	9.1	6.9
estimated pore dimension, N linker−N linker (Å)		8.5	7.9	6.0	3.4, 2.6	3.0, 3.7	6.7	6.9
		N_2 Adsorption Data						
maximum volume adsorbed (cm^3/g STP)		11.7		16.5		5.7	6.8	
corresponding pressure (Torr)		757		750		755	762	
Langmuir surface area (m^2/g)		40		107		18	36	

[a] N linker−N linker is the distance of C(7)−C(8′) for **5a**, **5b**, and **7**, C(8)−C(8′) for **6** and **8**, C(8)−C(9′) for **9**, and N(2)−N(2′) for **10**. [b] N linker conformation and dihedral angle are O(2)−C(7)−C(8)−O(3) for **5a**, **5b**, and **7**, O(2)−C(7)−C(8)−C(9) and C(7)−C(8)−C(9)−O(3) for **6** and **8**, and O(2)−C(7)−C(10)−O(3) for **9**. [c] Pd(1)−N(3′) for **10**. [d] Angle specified by P(1)−M−N, where N is a nitrogen atom that is located at the cis-position relative to P(1), and so forth. [e] The oxygen atoms O(5), O(6), and O(7) belong to one triflate counterion and O(8), O(9), and O(10) to another.

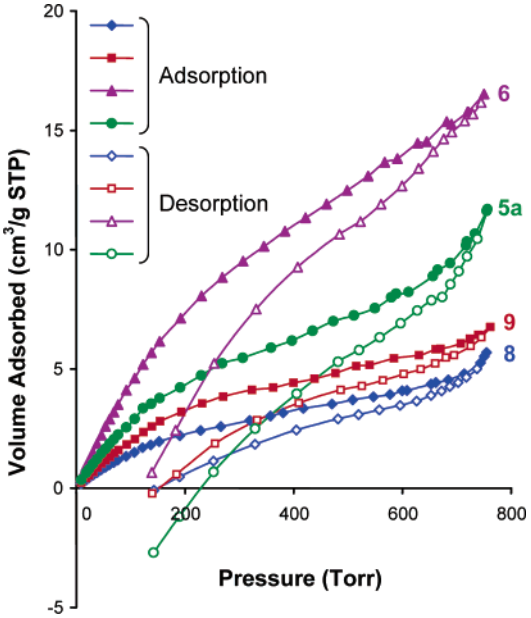

Figure 10. Adsorption isotherms for N_2 on desolvated polycrystalline compounds of **5a**, **6**, **8**, and **9** at 77 K. Filled and unfilled data points indicate adsorption and desorption, respectively.

rapid adsorption of N_2 was observed with pronounced hysteresis upon desorption. A polycrystalline sample of **5a** showed the second highest adsorption (11.7 cm^3/g STP of N_2 at 757 Torr) and exhibited hysteresis between its adsorption and desorption as well. Polycrystalline samples of **8** and **9** adsorbed 5.7 and 6.8 cm^3/g STP of N_2 at 755 and 762 Torr, respectively, significantly less than **5a** and **6**; however, both **8** and **9** also exhibit hysteresis.

Discussion

The flexible linkers (**1**−**4**) in this study have different lengths and conformational degrees of freedom. They provided an opportunity to examine the effects of flexibility in coordination-directed self-assembly. We utilized the ester moiety to link a variety of spacer units with pyridyl groups that can bind to metal units. The use of ester linkages provided several advantages, such as stability, ease of synthesis, and a simple but useful functional group. Esters also have the added advantage of being hydrogen bond acceptors. Assemblies containing such groups could exhibit host−guest properties based on hydrogen bonding.

Incorporating flexible linkers in porous molecular materials could generate ensembles where the flexibility of the linkers might be transferred to the supramolecular structure. Hence, we studied the structural changes that complex **5a** undergoes upon exchange with other solvents. When the nitromethane-containing crystal structure **5a** was recrystallized from a dichloromethane−toluene mixture, a new structure **5b** was obtained that incorporated toluene molecules instead of nitromethane molecules in the pore. X-ray analysis of structure **5b** reveals that the flexible framework undergoes a slight conformational change in the C(6)−O(2)−C(7)−C(8) dihedral angle from 154.5° in

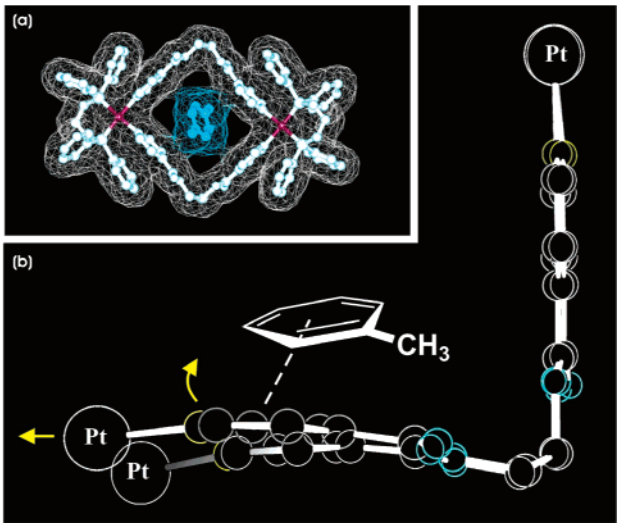

Figure 11. (a) Enclathrated toluene molecule in **5b** is held via $\pi-\pi$ stacking interactions. (b) The flexible linker framework in **5b** underwent conformational change from **5a**.

5a to 160.2° in **5b**, to form strong $\pi-\pi$ stacking interactions (3.6 Å) between the pyridyl groups and the toluene molecules (Figure 11). This suggests that the flexibility of the linker **1** was transferred to the solid-state structures of **5a** and **5b**. Similar behavior has been observed with other flexible spacer units in coordination networks.[14b]

Analyses of the X-ray crystal structures of **5a**, **5b**, and **6**−**10** reveal that the metallacycles stack along one or two of the crystallographic axes, forming nanopore channels. The shape and topology of the nanopores are largely determined by the flexible linkers, the metal units with phosphorus ligands, and the stacking of the metallacycles. To determine the pore dimensions, the factors that need to be considered are the tilting of the metallacycles with respect to their stacking axes and the ionic and van der Waals radii. The pore dimensions are estimated by projecting the cavity of the metallacycles to the plane perpendicular to the stacking axes and then subtracting the ionic and van der Waals radii from the distances of M−M and N linker−N linker, respectively, in the projected images (Table 2). The pores of **5a** and **5b** are along the *c*-axis, and the layers of the metallacycles are parallel to the *ab*-plane. Two adjacent layers are shifted by half of the dimensions of the *ab*-plane of the unit cell (Figure 12). Thus, in this alternating stacking manner, the pores in the crystals of **5a** and **5b** are formed by every second layer of the metallacycles, resulting in significantly larger stacking distances between metallacycles forming a given channel (19.1 Å for **5a** and 19.0 Å for **5b**). The actual pore size is effectively reduced from the estimated values (10.8 Å × 8.5 Å for **5a**) because the two adjacent layers of metallacycles partially block each other's pore. The crystal of **5a** contains six nitromethane molecules per metallacycle; five were found inside the pore, and one was found outside. The crystal of **5b** contains three toluene molecules with 50% occupancy per metallacycle. One toluene molecule is present within each metallacycle, while the other two are between adjacent metallacycles. In contrast to the stacking of alternating layers in **5a** and **5b**, **6** has the layers of metallacycles aligned; i.e., the cavities are right on top of each other (Figure 13). As a result, the pore dimensions of **6** remain reasonably large without a significant reduction from the estimated values (8.9 Å × 6.0 Å). The crystal of **6** contains two water and two methanol molecules per metallacycle; the water molecules are found inside the pore, whereas the methanol molecules are located outside. The complexes **7** and **8** have nanopores along the crystallographic axes *a* and *b* (Figure 14). However, this requires approximately a 45° tilt from the two axes, thus resulting in very narrow pores in the N linker−N linker direction (for **7**, 3.4, 2.6 Å; for **8**, 3.0, 3.7 Å). The cavities of **7** and **8** are filled with one nitromethane and one diethyl ether molecule, respectively. The estimated pore dimensions of **9** are fairly large (9.1 Å × 6.7 Å), and the metallacyclic layers are aligned, but the phenyl groups of the (dppp) moieties block a large proportion of the pore and this reduces the overall porosity of the crystal (Figure 15). One methanol molecule per metallacycle is found inside the pore of **9**. The crystal structure of **10** indicates two nitromethane molecules per metallacycle are located outside of the pore.

To assess the porous properties of the crystalline materials, we carried out N_2 adsorption studies at 77 K. Prior to the experiments, the samples were placed under vacuum until no

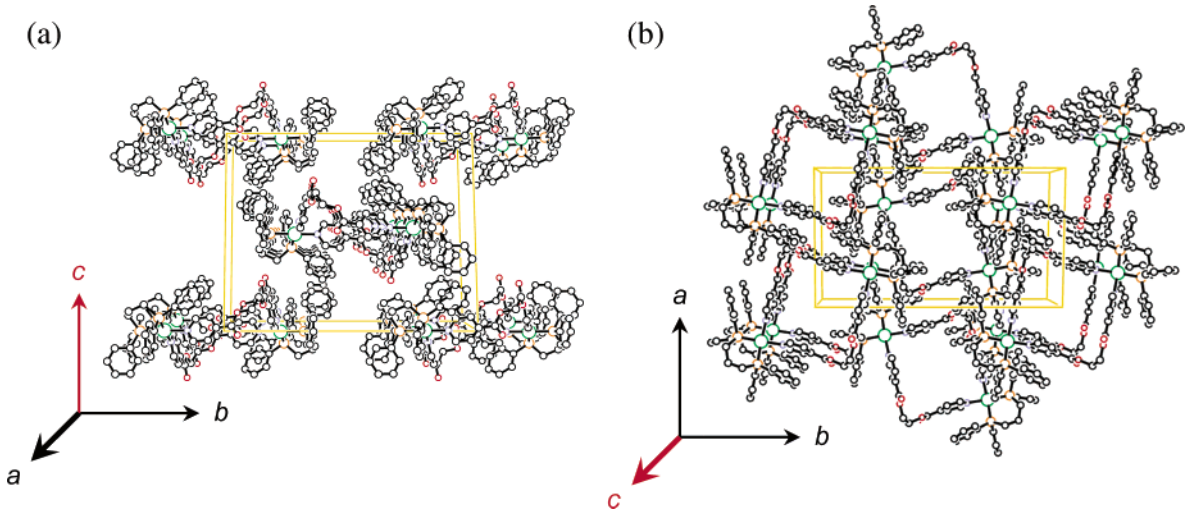

Figure 12. Packing diagram of **5a**. The red arrow indicates the direction of the pores (*c*-axis). (a) Viewed along the *a*-axis. The two adjacent layers of metallcycles **5** are shifted by half of the dimensions of the *ab*-plane of the unit cell. (b) Viewed along the *c*-axis. The partially blocked pore caused by the alternating positions of the layers can be observed (center of the picture).

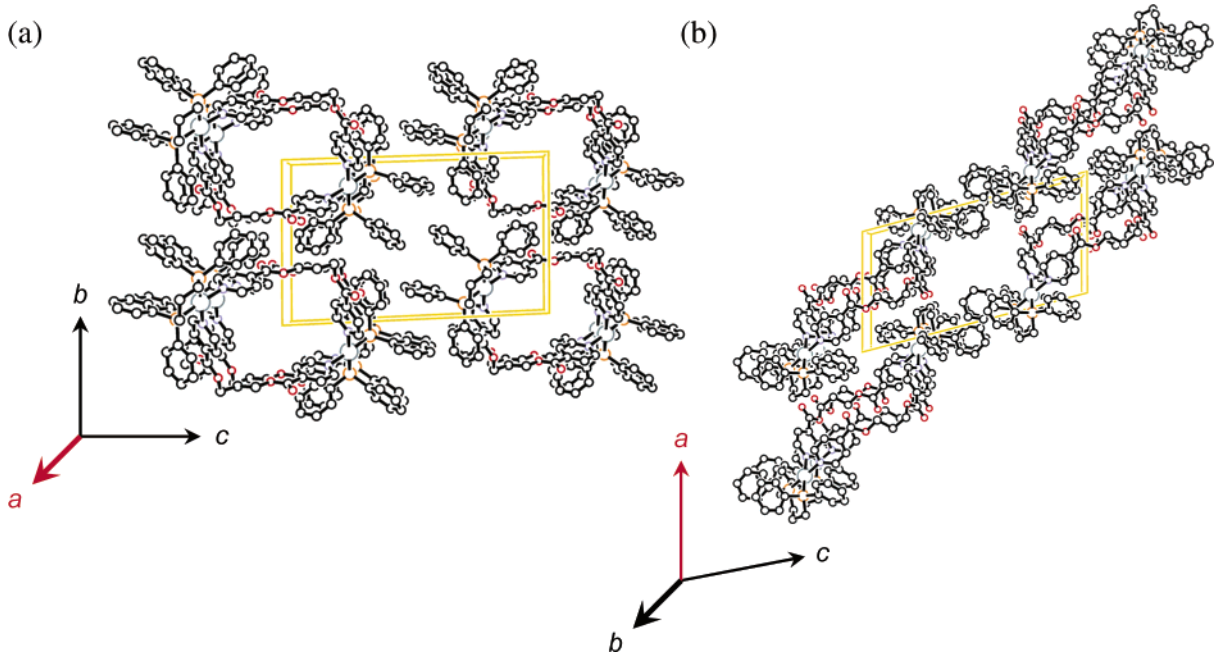

Figure 13. Packing diagram of **6**. The red arrow indicates the direction of the pores (*a*-axis). (a) Viewed along the *a*-axis. (b) Viewed along the *b*-axis. The layers of the metallacycles **6** are aligned; as a result, the cavities are right on top of each other.

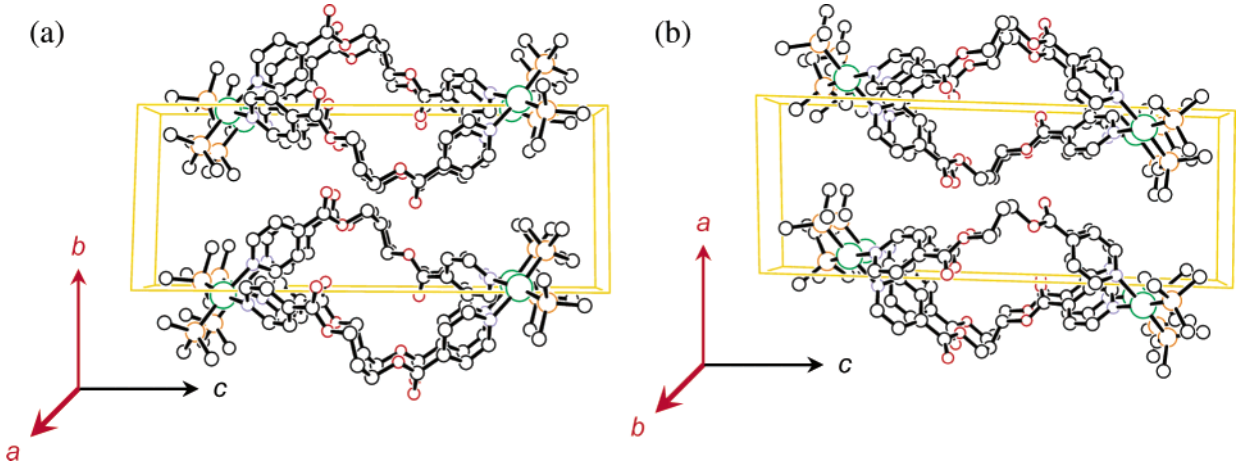

Figure 14. Packing diagram of **8**. The directions of the pores are indicated in red. This crystal forms pores that can be seen from two directions (*a*- and *b*-axes). However, in both directions, the pores are quite narrow, and the dimensions in the N linker−N linker directions are short. (a) Viewed along the *a*-axis. (b) Viewed along the *b*-axis.

further weight loss from solvent evaporation was observed. The experiment was repeated several times for each sample to reproduce the isotherm. As shown in Figure 10, complexes **5a**, **6**, **8**, and **9** exhibit N_2 adsorption with pronounced hysteresis upon desorption. The rapid rise followed by a monotonically increasing curve at low pressure is indicative of uniform pore size distribution and is characteristic of other nanoporous materials.[18,19] The pronounced hysteresis may have arisen from capillary condensation within the crystals.[18] Moreover, the desorption in these crystals is unusual since it releases the absorbed N_2 quite rapidly as pressure decreases. This behavior might arise from structural strain built up during the adsorption, possibly due to the flexibility of the linker frameworks. For this reason, no isotherm plots from the crystals fit any IUPAC classifications.[20]

Sample **6** exhibits the greatest N_2 adsorption with 16.5 cm^3/g STP (750 Torr), and the Langmuir surface area for **6** was calculated to be 107 m^2/g.[21] Clearly this is due to the effective stacking of the aligned layers of the metallacycles (Figure 13)

(18) Sigmoidal isotherms are observed when guest-inclusion is accompanied by phase changes. For complete discussion see: (a) Dewa, T.; Endo, K.; Aoyama, Y. *J. Am. Chem. Soc.* **1998**, *120*, 8933−8940. (b) Dewa, T.; Aoyama, Y. *Chem. Lett.* **2000**, 854−855. (c) Ariga, K.; Endo, K.; Aoyama, Y.; Okahata, Y. *Colloids Surf., A* **2000**, *169*, 177−186. (d) Matsuura, K.; Ariga, K.; Endo, K.; Aoyama, Y.; Okahata, Y. *Chem.-Eur. J.* **2000**, *6*, 1750−1756. (e) Dewa, T.; Saiki, T.; Imai, Y.; Endo, K.; Aoyama, Y. *Bull. Chem. Soc. Jpn.* **2000**, *73*, 2123−2127. (f) Naito, M.; Sasaki, Y.; Dewa, T.; Aoyama, Y.; Okahata, Y. *J. Am. Chem. Soc.* **2001**, *123*, 11037−11041.

(19) (a) Fletcher, A. J.; Cussen, E. J.; Prior, T. J.; Rosseinsky, M. J.; Kepert, C. J.; Thomas, K. M. *J. Am. Chem. Soc.* **2001**, *123*, 10001−10011. (b) Kepert, C. J.; Prior, T. J.; Rosseinsky, M. J. *J. Am. Chem Soc.* **2000**, *122*, 5158−5168. (c) Rujiwatra, A.; Kepert, C. J.; Claridge, J. B.; Rosseinsky, M. J.; Kumagai, H.; Kurmoo, M. *J. Am. Chem. Soc.* **2001**, *123*, 10584−10594. (d) Li, H.; Eddaoudi, M.; Groy, T. L.; Yaghi, O. M. *J. Am. Chem. Soc.* **1998**, *120*, 8571−8572. (e) Reineke, T. M.; Eddaoudi, M.; O'Keeffe, M.; Yaghi, O. M. *Angew. Chem., Int. Ed.* **1999**, *38*, 2590−2594. (f) Eddaoudi, M.; Li, H.; Yaghi, O. M. *J. Am. Chem. Soc.* **2000**, *122*, 1391−1397. (g) Chen, B.; Eddaoudi, M.; Hyde, S. T.; O'Keeffe, M.; Yaghi, O. M. *Science* **2001**, *291*, 1021−1023.

(20) Sing, K. S. W.; Everett, D. H.; Haul, R. A. W.; Moscou, L.; Pierotti, R. A.; Rouquérol, J.; Siemieniewska, T. *Pure Appl. Chem.* **1985**, *57*, 603−619.

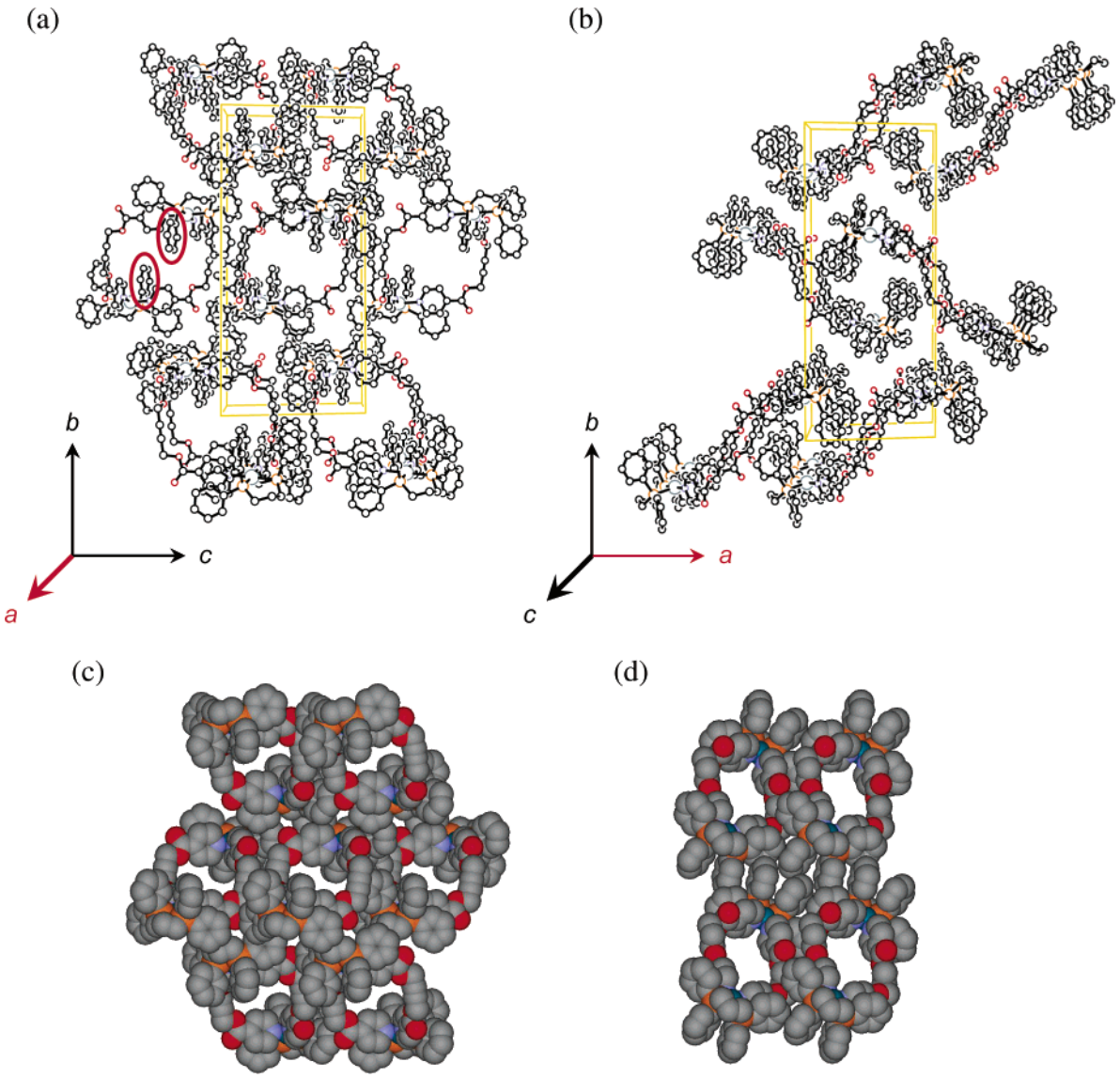

Figure 15. (a) Packing diagram of **9** viewed along the *a*-axis. The directions of the pores are indicated in red. Although this crystal forms pores along the *a*-axis, the phenyl groups of dppp block a large proportion of the pores (shown in red ovals). (b) Viewed along the *c*-axis. (c) CPK representation of the packing diagram of **9** viewed along the *a*-axis. This view illustrates the pore blockage by the phenyl groups. (d) CPK respresentation of **6** showing the unblocked pores resulting in the highest N_2 adsorption.

and the reasonably large pore dimensions (8.9 Å × 6.0 Å, Table 2). Crystals of **5a** had the second highest N_2 adsorption of 11.7 cm^3/g STP (757 Torr) with 40 m^2/g of Langmuir surface area. Although this complex has fairly large estimated pore dimensions (10.8 Å × 8.5 Å), the alternating layers of the metallacycles in **5a** are not as effective at adsorbing N_2 as the aligned layer crystals of **6** are (Figure 12). Assemblies **8** and **9** adsorbed significantly less N_2 than **5a** and **6**. Although the pores in **8** can be seen along the *a*- and *b*-axes, they are very narrow (13.0 Å × 3.0 Å along the *a*-axis and 13.1 Å × 3.7 Å along the *b*-axis) (Figure 14). Considering the dimensions of an N_2 molecule, this material was expected to be inefficient at N_2 adsorption. Indeed, **8** adsorbed only 5.7 cm^3/g STP (755 Torr) with an 18 m^2/g Langmuir surface area. The estimated pore dimensions of **9** are relatively large (9.1 Å × 6.7 Å), but its N_2 adsorption was only 6.8 cm^3/g STP (762 Torr). In the packing of **9**, the phenyl groups of the (dppp) moieties block a large proportion of the pores in the crystal (Figure 15). Although N_2 is restricted from going into these pores, the surface area should be available because the pores are partially blocked but not completely filled. Thus, a Langmuir surface area of 36 m^2/g for **9** was calculated, which is twice as large as that of **8**.

Conclusion

A family of discrete metallacycles that comprise flexible organic components of various lengths and conformational degrees of freedom were synthesized via self-assembly. The flexible ditopic linkers used (**1**−**4**) contain ester linkages that join two pyridyl groups at each end of a spacer unit. Upon reaction with ditopic cis-square-planar metal units, supramolecular metallacycle structures (**5**−**10**) formed and were fully characterized in both solution and the solid states. The crystal structures reveal that the metallacycles are stacked along one or two of the crystallographic axes, forming nanoscopic pores. Polycrystalline samples of **5a**, **6**, **8**, and **9** exhibit nanoporous properties and adsorbed 11.7, 16.5, 5.7, and 6.8 cm^3/g STP of

(21) Gregg, S. J.; Sing, K. S. W. *Adsorption, Surface Area and Porosity*, 2nd ed.; Academic Press: London, UK, 1982.

N_2, respectively. The trend of N_2 adsorption can be explained by the estimated pore sizes and packing of the metallacycles. X-ray studies on the exchange of nitromethane solvent molecules for toluene reveals that the flexible framework of **5** can undergo a conformational change to maximize interactions with the newly introduced guest. Our work demonstrates that metallacycles with ditopic flexible linkers allow the formation of zeolite-like frameworks with custom-designed pore sizes and molecular topologies.

Experimental Section

General. Isonicotinoyl chloride hydrochloride, ethylene glycol, 1,3-propanediol, 2-butyne-1,4-diol, 2,6-pyridinedicarboxylic acid chloride, and 4-pyridinemethanol were used as received from commercial sources (Sigma-Aldrich or Lancaster). All solvents were distilled using standard methods prior to use. NMR spectra were obtained at room temperature with a Varian XL-300 spectrometer. The ^{1}H NMR spectra were recorded at 300 MHz, and the chemical shifts were reported relative to those of the residual protons in the deuterated solvents, δ 7.27 and 4.33 ppm in $CDCl_3$ and CD_3NO_2, respectively. The $^{13}C\{^1H\}$ NMR spectra were recorded at 75 MHz, and the chemical shifts were reported relative to that of the ^{13}C in $CDCl_3$ (δ 77.2 ppm). The ^{19}F and $^{31}P\{^1H\}$ NMR spectra were recorded at 282 and 121 MHz, respectively, and the chemical shifts were reported relative to those of external standards of $CFCl_3$ and H_3PO_4, respectively (δ 0.0 ppm in each case). Elemental analysis was performed by Atlantic Microlab Inc. (Norcross, GA). Single-crystal X-ray diffraction data for all compounds were collected on a Nonius KappaCCD diffractometer equipped with Mo Kα radiation (λ = 0.71073 Å) at 150(1) K. The structures were solved by a combination of direct and heavy-atom methods using SIR 97. SHELXL97 was used for the final structural refinement. ESI-MS spectra were recorded on a Micromass Quattro II triple-quadrupole mass spectrometer with Micromass MassLynx software. Adsorption isotherms were measured with a Micromeritics ASAP 2010 surface area and porosimetry analyzer. The polycrystalline samples were degassed overnight and then loaded onto the instrument. N_2 (99.9995%) was incrementally dosed into the sample tubes to provide the adsorption measurements. The experiment was carried out at 77 K. Calculation of surface area was carried out according to the literature.[22]

1,2-Ethanediyl Di-4-pyridinecarboxylate (1). To a stirred mixture of isonicotinoyl chloride hydrochloride (513 mg, 2.88 mmol) in anhydrous dichloromethane (50 mL) at room temperature was added triethylamine (0.82 mL, 5.9 mmol). Subsequently, ethylene glycol (85.0 mg, 1.37 mmol) was added to the reaction, and the mixture was refluxed for 12 h. After the mixture was washed with saturated aqueous sodium bicarbonate solution (20 mL), the organic phase was dried over anhydrous potassium carbonate and filtered. Removal of the solvent gave **1**. Yield: 305 mg (82%). ^{1}H NMR ($CDCl_3$): δ (ppm) 8.79 (dd, J = 4.4, 1.7 Hz, 4H, PyH_α), 7.85 (dd, J = 4.4, 1.5 Hz, 4H, PyH_β), 4.72 (s, 4H, CH_2). $^{13}C\{^1H\}$ NMR ($CDCl_3$): δ (ppm) 165.1 (C=O), 150.9 (PyC_α), 137.0 (PyC_γ), 123.0 (PyC_β), 63.4 (CH_2). Anal. Calcd for $C_{14}H_{12}N_2O_4$: C, 61.76; H, 4.44; N, 10.29. Found: C, 61.40; H, 4.40; N, 10.08.

1,3-Propanediyl Di-4-pyridinecarboxylate (2). Compound **2** was prepared in a manner similar to that used for **1**, except that 1,3-propanediol (107 mg, 1.41 mmol) was used in the reaction. Yield: 350 mg (87%). ^{1}H NMR ($CDCl_3$): δ (ppm) 8.79 (dd, J = 4.4, 1.6 Hz, 4H, PyH_α), 7.84 (dd, J = 4.4, 1.7 Hz, 4H, PyH_β), 4.55 (t, J = 6.3 Hz, 4H, OCH_2), 2.31 (quintet, J = 6.2 Hz, 2H, OCH_2CH_2). $^{13}C\{^1H\}$ NMR ($CDCl_3$): 165.1 (C=O), 150.8 (PyC_α), 137.2 (PyC_γ), 122.9 (PyC_β), 62.5 (OCH_2), 28.1 (OCH_2CH_2). Anal. Calcd for $C_{15}H_{14}N_2O_4$: C, 62.93; H, 4.93; N, 9.79. Found: C, 62.83; H, 4.81; N, 9.57.

(22) Webb, P. A.; Orr, C. *Analytical Methods in Fine Particle Technology*; Micromeritics: Norcross, GA, 1997.

2-Butyne-1,4-diyl Di-4-pyridinecarboxylate (3). Compound **3** was prepared in a manner similar to that used for **1**, except that 2-butyne-1,4-diol (103 mg, 1.20 mmol) was used. Yield: 300 mg (85%). ^{1}H NMR ($CDCl_3$): δ (ppm) 8.82 (bd, J = 5.6 Hz, 4H, PyH_α), 7.89 (bd, J = 5.9 Hz, 4H, PyH_β), 5.03 (s, 4H, CH_2). $^{13}C\{^1H\}$ NMR ($CDCl_3$): δ (ppm) 164.6 (C=O), 150.9 (PyC_α), 136.7 (PyC_γ), 123.1 (PyC_β), 81.1 (C≡C), 53.4 (CH_2). Anal. Calcd for $C_{16}H_{12}N_2O_4$: C, 64.86; H, 4.08; N, 9.45. Found: C, 64.40; H, 4.07; N, 9.18.

Bis(4-pyridylmethyl) Pyridine-2,6-dicarboxylate (4). To a stirred mixture of 2,6-pyridinedicarboxylic acid chloride (510 mg, 2.50 mmol) in anhydrous dichloromethane (50 mL) and triethylamine (0.72 mL, 5.2 mmol) was added 2 equiv of 4-pyridinemethanol (560 mg, 5.13 mmol), and the mixture was refluxed for 12 h. Following a workup similar to that used for **1**, **4** was obtained. Yield: 786 mg (90%). ^{1}H NMR ($CDCl_3$): δ (ppm) 8.64 (bd, J = 5.9 Hz, 4H, PyH_α), 8.36 (d, J = 7.6 Hz, 2H, pyridyleneH_β), 8.08 (t, J = 7.8 Hz, 1H, pyridyleneH_γ), 7.40 (bd, J = 5.6 Hz, 4H, PyH_β), 5.49 (s, 4H, CH_2). $^{13}C\{^1H\}$ NMR ($CDCl_3$): δ (ppm) 164.3 (C=O), 150.4 (PyC_α), 148.2 (pyridyleneC_α), 144.5 (PyC_γ), 138.8 (pyridyleneC_γ), 128.6 (pyridyleneC_β), 122.2 (PyC_β), 65.9 (CH_2). Anal. Calcd for $C_{19}H_{15}N_3O_4$: C, 65.32; H, 4.33; N, 12.03. Found: C, 64.92; H, 4.35; N, 11.93.

[(dppp)Pt(1)]$_2$(OTf)$_4$ (5). A 1.0 mL nitromethane-d_3 solution of (dppp)Pt(OTf)$_2$ (3.57 mg, 3.94 μmol) was added to **1** (1.08 mg, 3.97 μmol) and stirred for 10 min at ambient temperature. The solvent volume was reduced, and **5** was precipitated by addition of diethyl ether. The resulting white solid was dried under vacuum. Yield: 4.45 mg (90%). ^{1}H NMR (CD_3NO_2): δ (ppm) 8.88 (bd, J = 6.1 Hz, 8H, PyH_α), 7.74−7.42 (m, 40H, PhH), 7.65 (bd, J = 6.6 Hz, 8H, PyH_β), 4.55 (s, 8H, OCH_2), 3.33 (m, 8H, PCH_2), 2.41 (m, 4H, PCH_2CH_2). $^{31}P\{^1H\}$ NMR (CD_3NO_2): δ (ppm) −13.1 (s, J_{P-Pt} = 3015 Hz). ^{19}F NMR (CD_3NO_2): δ (ppm) −78.5. Anal. Calcd for $C_{86}H_{76}F_{12}N_4O_{20}P_4Pt_2S_4\cdot 2(CH_3CH_2)_2O$: C, 45.09; H, 3.86; N, 2.24; S, 5.12. Found: C, 45.34; H, 3.98; N, 2.45; S, 5.10.

[(dppp)Pt(1)]$_2$(OTf)$_4$·6Nitromethane (5a). Compound **5** was dissolved in nitromethane (ca. 1 mM), and diethyl ether was diffused into the solution for 2 days, affording **5a** as X-ray quality crystals.

[(dppp)Pt(1)]$_2$(OTf)$_4$·1.5Toluene (5b). Compound **5a** was redissolved in a mixture of dichloromethane−toluene (90:10), and the solution was allowed to slowly evaporate at room temperature. After 24 h, X-ray quality crystals of **5b** were obtained.

[(dppp)Pd(2)]$_2$(OTf)$_4$ (6). A 1.0 mL nitromethane-d_3 solution of (dppp)Pd(OTf)$_2$ (2.94 mg, 3.60 μmol) was added to **2** (1.03 mg, 3.60 μmol) and stirred for 10 min at ambient temperature. The solvent volume was reduced, and **6** was precipitated by addition of diethyl ether. The resulting white solid was dried under vacuum. Yield: 3.94 mg (98%). Compound **6** was then redissolved in methanol (ca. 1 mM), and diethyl ether was diffused into the solution for 2 days, affording X-ray quality crystals. ^{1}H NMR (CD_3NO_2): δ (ppm) 8.75 (bd, J = 5.1 Hz, 8H, PyH_α), 7.70−7.35 (m, 40H, PhH), 7.54 (bd, J = 6.4 Hz, 8H, PyH_β), 4.31 (t, J = 5.3 Hz, 8H, OCH_2), 3.25 (m, 8H, PCH_2), 2.43 (m, 4H, PCH_2CH_2), 2.14 (quintet, J = 5.3 Hz, 4H, OCH_2CH_2). $^{31}P\{^1H\}$ NMR (CD_3NO_2): δ (ppm) 9.5 (s). ^{19}F NMR (CD_3NO_2): δ (ppm) −78.7. Anal. Calcd for $C_{88}H_{80}F_{12}N_4O_{20}P_4Pd_2S_4\cdot 2H_2O$: C, 47.13; H, 3.78; N, 2.50; S, 5.72. Found: C, 46.96; H, 3.83; N, 2.57; S, 5.65.

[(Me$_3$P)$_2$Pt(1)]$_2$(OTf)$_4$ (7). A 2.0 mL nitromethane-d_3 solution of *cis*-(Me$_3$P)$_2$Pt(OTf)$_2$ (4.75 mg, 7.36 μmol) was added to **1** (1.98 mg, 7.27 μmol) and stirred for 10 min at ambient temperature. The solvent volume was reduced, and **7** was precipitated by addition of diethyl ether. The resulting white solid was dried under vacuum. Yield: 6.40 mg (96%). Compound **7** was then redissolved in nitromethane (ca. 1 mM), and diethyl ether was diffused into the solution for 7 days, affording X-ray quality crystals. ^{1}H NMR (CD_3NO_2): δ (ppm) 9.11 (bd, J = 4.4 Hz, 8H, PyH_α), 8.15 (bd, J = 5.9 Hz, 8H, PyH_β), 4.71 (s, 8H, OCH_2), 1.65 (d, J_{H-P} = 11.2 Hz, 36H, P(CH_3)$_3$). $^{31}P\{^1H\}$ NMR (CD_3NO_2): δ (ppm) −27.9 (s, J_{P-Pt} = 3150 Hz). ^{19}F NMR (CD_3NO_2):

δ (ppm) −78.7. Anal. Calcd for $C_{44}H_{60}F_{12}N_4O_{20}P_4Pt_2S_4$: C, 28.80; H, 3.30; N, 3.05; S, 6.99. Found: C, 29.02; H, 3.72; N, 3.29; S, 6.89.

[(Me$_3$P)$_2$Pt(2)]$_2$(OTf)$_4$ (8). A 2.0 mL nitromethane-d_3 solution of *cis*-(Me$_3$P)$_2$Pt(OTf)$_2$ (4.61 mg, 7.14 μmol) was added to **2** (2.04 mg, 7.13 μmol) and stirred for 10 min at ambient temperature. The solvent volume was reduced, and **8** was precipitated by addition of diethyl ether. The resulting white solid was dried under vacuum. Yield: 6.31 mg (88%). Compound **8** was then redissolved in nitromethane (ca. 1 mM), and diethyl ether was diffused into the solution for 7 days, affording X-ray quality crystals. ^{1}H NMR (CD_3NO_2): δ (ppm) 9.04 (bd, J = 4.4 Hz, 8H, PyH_α), 8.09 (bd, J = 6.1 Hz, 8H, PyH_β), 4.49 (t, J = 5.5 Hz, 8H, OCH_2), 2.29 (quintet, J = 5.2 Hz, 4H, OCH$_2$CH_2), 1.67 (d, J_{H-P} = 11.2 Hz, 36H, P(CH_3)$_3$). ^{31}P{^{1}H} NMR (CD_3NO_2): δ (ppm) −27.9 (s, J_{P-Pt} = 3147 Hz). ^{19}F NMR (CD_3NO_2): δ (ppm) −78.7. Anal. Calcd for $C_{46}H_{64}F_{12}N_4O_{20}P_4Pt_2S_4\cdot CH_3NO_2\cdot(CH_3CH_2)_2O\cdot H_2O$: C, 30.38; H, 3.95; N, 3.47; S, 6.36. Found: C, 30.13; H, 3.80; N, 3.19; S, 6.66.

[(dppp)Pd(3)]$_2$(OTf)$_4$ (9). A 2.5 mL nitromethane-d_3 solution of (dppp)Pd(OTf)$_2$ (24.05 mg, 29.44 μmol) was added to **3** (8.72 mg, 29.4 μmol) and stirred for 10 min at ambient temperature. The assembly **9** was precipitated by addition of diethyl ether. The resulting white solid was dried under vacuum. Yield: 30.77 mg (94%). Compound **9** was then redissolved in methanol (ca. 1 mM), and diethyl ether was diffused into the solution for 2 days, affording X-ray quality crystals. ^{1}H NMR (CD_3NO_2): δ (ppm) 8.87 (bd, J = 5.4 Hz, 8H, PyH_α), 7.73−7.39 (m, 40H, PhH), 7.60 (bd, J = 5.4 Hz, 8H, PyH_β), 4.90 (s, 8H, OCH_2), 3.27 (m, 8H, PCH_2), 2.46 (m, 4H, PCH$_2$CH_2). ^{31}P{^{1}H} NMR (CD_3NO_2): δ (ppm) 9.3 (s). ^{19}F NMR (CD_3NO_2): δ (ppm) −78.5. Anal. Calcd for $C_{90}H_{76}F_{12}N_4O_{20}P_4Pd_2S_4$: C, 48.55; H, 3.44; N, 2.52; S, 5.76. Found: C, 48.42; H, 3.73; N, 2.62; S, 5.48.

[(dppp)Pd(4)]$_2$(OTf)$_4$ (10). A 4.0 mL nitromethane-d_3 solution of (dppp)Pd(OTf)$_2$ (9.83 mg, 12.0 μmol) was added to **4** (4.05 mg, 11.6 μmol) and stirred for 10 min at ambient temperature. NMR spectra showed two distinguishable species in equilibrium. The solvent volume was reduced, and **10** was precipitated by addition of diethyl ether. The resulting white solid was dried under vacuum. Yield: 13.0 mg (91%). Compound **10** was then redissolved in nitromethane (ca. 1 mM), and diethyl ether was diffused into the solution for 2 days, affording X-ray quality crystals. Although two species were observed in solution, only the dimeric species crystallized. ^{1}H NMR (CD_3NO_2): δ (ppm) 8.65 (bd, J = 5.1 Hz, PyH_α), 8.57 (bd, J = 4.9 Hz, PyH_α), 8.36−8.09 (m, pyridylene$H_{\beta,\gamma}$), 8.36−8.09 (m, pyridylene$H_{\beta,\gamma}$), 7.82−7.38 (m, PhH), 7.71−7.38 (m, PhH), 7.29 (bd, J = 6.2 Hz, PyH_β), 7.19 (bd, J = 5.9 Hz, PyH_β), 5.29 (s, OCH_2), 5.01 (s, OCH_2), 3.25 (m, PCH_2), 3.25 (m, PCH_2), 2.47 (m, PCH$_2$CH_2), 2.39 (m, PCH$_2$CH_2). ^{31}P{^{1}H} NMR (CD_3NO_2): δ (ppm) 10.8 (s), 9.3 (s). ^{19}F NMR (CD_3NO_2): δ (ppm) −78.6. ESI-MS: m/z 2183.0 (calcd for {[(dppp)Pd(**4**)]$_2$(OTf)$_3$}$^+$ 2183.2), 1600.3 (calcd for {[(dppp)Pd(**4**)]$_3$(OTf)$_4$}$^{2+}$ 1600.1). Anal. Calcd for $C_{96}H_{82}F_{12}N_6O_{20}P_4Pd_2S_4\cdot CH_3NO_2\cdot(CH_3CH_2)_2O$: C, 49.16; H, 3.88; N, 3.97; S, 5.20. Found: C, 49.53; H, 3.86; N, 3.61; S, 5.38.

Acknowledgment. Financial support by the National Science Foundation (CHE-0306720), the National Institutes of Health (GM-57052), and an NIH Postdoctoral Fellowship (Grant GM66504-01) for J.C.N. is gratefully acknowledged. Work by the ELORET authors is supported by a NASA contract. We thank Dr. C. Addicott and Dr. E. Rachlin for assistance with mass spectrometry.

Supporting Information Available: Crystallographic data for **5a**, **5b**, and **6**−**10** (CIF); NMR spectra (^{1}H and ^{13}C{^{1}H} for **1**−**4**; ^{1}H and ^{31}P{^{1}H} for **5**−**10**) and ESI-MS spectra for {[(dppp)Pd(**4**)]$_2$(OTf)$_3$}$^+$ and {[(dppp)Pd(**4**)]$_3$(OTf)$_4$}$^{2+}$ (PDF). This material is available free of charge via the Internet at http://pubs.acs.org.

JA0388919